Hindawi
Advances in Civil Engineering
Volume 2024, Article ID 3685857, 15 pages
https://doi.org/10.1155/2024/3685857

*Research Article*

# Experimental Study on Shear Characteristics of Coal Samples in Different Water-Bearing States

**Yang Wu ,[1,2] Lujun Wang ,[1] Baoyang Wu,[1] and Ze Xia [3]**

[1]*State Key Laboratory of Water Resource Protection and Utilization in Coal Mining, National Institute of Clean and Low Carbon Energy, Beijing 102211, China*
[2]*Guoneng Shendong Coal Technology Research Institute, Yulin 719000, China*
[3]*School of Mines, China University of Mining and Technology, Xuzhou 221116, China*

Correspondence should be addressed to Yang Wu; wuyangln@163.com

Received 6 September 2023; Revised 18 November 2023; Accepted 27 December 2023; Published 20 January 2024

Academic Editor: Dawei Yin



During the establishment of the coal mine goaf reservoir, the strength of the coal pillar dam was weakened by various water–rock interactions triggered by water movement. To explore the influence of the water-bearing state on the shear characteristics of coal pillar dams, the 2–2 coal seam of Shangwan Coal Mine in the Shendong Mining area was taken as the research object and was prepared to coal samples with different moisture contents and different drying-saturation cycles, and the variable angle shear test of coal samples was carried out. The law of water absorption of coal samples under natural and pressurized conditions is obtained. The research results show that the shear characteristics of coal samples change significantly under the action of water, with the increase of moisture content and drying-saturation cycles, the lower the shear strength of coal samples is, the larger the peak shear strain is, and the cohesion and internal friction angle of coal samples decrease linearly. According to the relationship between cohesion, internal friction angle, moisture content, and drying-saturation cycle times, the Mohr–Coulomb model of coal samples considering moisture content and immersion times is established, which contributes to the load-bearing capacity estimation of water-bearing coal mass. Additionally, scanning electron microscope analysis revealed significant changes in the microstructure of coal samples under different moisture states: as the moisture content and dry-saturation cycles increase, the microstructure of the coal samples gradually transforms from orderly and compact to disordered and murky, elucidating the mechanism by which moisture weakens the mechanical properties of the coal samples. The research results provide a useful reference for engineering problems related to the stability evaluation of coal bodies involving the repeated erosion effect of water.

## 1. Introduction

The ecologically fragile mining area in central and western China is a strategically important area for the development of coal resources in China [1]. This area is located in an arid and semi-arid area, and a water-scarce area where vegetation is sparse and soil erosion is serious. Coal mining activities will inevitably destroy the structural integrity of some underground rock formations and often destroy the underground aquifer, resulting in water level drop, surface water loss, surface vegetation damage, and surface water resource loss, which is even more serious [2]. Part of the water in the aquifer penetrates into various layers along the water-conducting fissures of the rock formation, causing a series of problems such as water seepage in the working face, water in the roadway, and water storage in the goaf, which puts forward new requirements for safe and efficient production. Hence, the conservation and utilization of groundwater resources during coal mining are necessary for achieving green coal mining [3, 4]. Water conservation mining [5, 6] and the widespread application of underground water reservoir technology [7–9] effectively solve the coal–water co-mining problem. However, underground reservoirs produce repeated infiltration and erosion effects of water on coal pillar dams during dynamic changes in water levels, which in turn produce repeated damage effects on coal pillar dam boundaries [10]. In addition, the disturbance of coal mining can lead to the destruction of overlying rock aquifers, causing water resources transport [11]. Moreover, water from some aquifers infiltrates into various layers along the hydraulic fissures of rock conduction, causing a series of problems such as water seepage at the working face, water drenching in the roadway, and water storage in the mining area [12, 13], which puts forward new requirements for safe and efficient production.

Water–rock interaction occurs in repeated water immersion and fractures water seepage in the coal column dams of underground reservoirs [14]. The process of water–rock interaction changes the microstructure, mineral components, and fracture development morphology of the coal rock body, which weakens the physical and mechanical properties of the coal rock body and easily causes deformation and instability of the engineered rock body [15]. Due to the differences in the structural composition of coal rock masses, the changes in mechanical properties after exposure to water have different regularities. Water can weaken the peak stress, elastic modulus, strain-softening modulus, and post-peak modulus of coal rock masses and reduce coal rock masses' shear strength, internal cohesion, and internal friction angle [10, 12, 16]. In engineering problems, shear damage is the most common form of damage. Shear load easily causes the destruction of different media connection surfaces, promotes fracture expansion and permeability change, and usually, shear damage destabilization occurs in a short period; the damage forms include three forms of shear damage, tensile and shear composite damage, and shear slip [17–21]. In order to evaluate the fracture development and expansion pattern during coal rock damage, acoustic emission monitoring technology has been widely used in the research work of rock mechanics [22–25]. Numerous scholars have studied the relationship between loading rate and the number of fractures, fracture types, and accumulated damage by monitoring the acoustic emission signals generated during the destruction of coal rock specimens under different loading conditions [26–30] and have studied the correlation of acoustic emission to locate fractures [31, 32].

The repeated erosion of coal by water has a non-negligible effect on the stability of engineering structures such as reservoir dams, roof slabs, and roadway envelopes. In this paper, the variations in shear strength and acoustic emission characteristics of coal samples under different dry-saturated cyclic water immersion states are investigated, exploring the deterioration laws of shear properties of coal samples in various water content states. Additionally, through scanning electron microscope (SEM) analysis, significant changes in the microstructure of coal samples under various moisture states are further revealed, and the mechanisms by which moisture content and drying-saturation cycling weaken the mechanical properties of coal samples are discussed. This investigation provides valuable references for engineering problems related to the stability evaluation of coal bodies subject to water's repeated erosive effect.

## 2. Experimental Program

*2.1. Selection and Preparation of Specimens.* In this paper, the 2–2 coal seam of Shangwan Coal Mine in the Shandong Mining Area of National Energy Group was selected as the research object. According to the requirements of the International Society of Rock Mechanics and the Geological and Mineral Industry Standard of the People's Republic of China, the selected rock specimens were sealed by wrapping in cling film and stored in a wooden box with foam at the bottom and around to reduce the damage caused by the rock during transportation and to maintain the original structure and moisture of the rock. During processing, the coal samples were processed into standard cubic specimens of $50 \times 50 \times 50$ mm along the laminae of the coal samples, with the error of the side length within $\pm 0.2$ mm and the nonparallelism of the two ends not exceeding 0.05 mm.

*2.2. Test Equipment.* The main test equipment and monitoring system are shown in Figure 1. The test equipment mainly includes drying, water immersion, stress loading, and acoustic emission signal acquisition systems.

(1) The vacuum constant temperature drying oven is selected to dry the coal sample. The vacuum environment greatly reduces the boiling point of the liquid inside the coal sample, which effectively shortens the drying time and avoids damage to the coal sample caused by the decomposition and oxidation of the coal sample components during the long drying process.
(2) The pressurized water immersion method is selected for coal sample immersion. The pressurized dipping device is mainly composed of a pressurized container, pressurized system, pressure protection device, and drainage unloading device, which can realize the simulation of the head pressure of the underground reservoir by adjusting the working pressure of the pressurized system. The maximum pressure applied to water can reach 3.0 MPa.
(3) The loading system adopts the MTS C64.106 electrohydraulic servo universal testing machine from the State Key Laboratory of Coal Resources and Safe Mining of China University of Mining and Technology. The test adopts displacement loading mode, and the loading rate is 0.1 mm/min.
(4) The acoustic emission signal acquisition system adopts the PCI-2 acoustic emission system of Physical Acoustic Corporation. The system mainly includes a control computer, amplifier, and acoustic emission sensor, which can realize the signal acquisition and data conversion when the rock material changes; the acoustic emission probe model used in the test is Nano30, with a resonant frequency of 140 kHz and frequency range of 125–750 kHz.

*2.3. Test Principle and Method.* The drying temperature of the drying oven was set to 105°C, and the specimen was dried. During the drying process, the coal sample was taken out and weighed every 20 min, and the coal sample was considered to have entered the drying state when the difference between the mass of the coal rock sample before and after twice was <0.01 g. After drying, the coal samples were tested for water absorption using a pressurized water


Figure 1: Schematic diagram of the experimental equipment: (a) electric blast drying oven; (b) immersion device; (c) servo universal testing machine; (d) shear indenter; (e) PCI-2 AE system.

immersion device. Since direct pressure soaking will cause the air inside the coal sample cannot be discharged in time and then cause the uneven distribution of water inside the coal sample. We divided the pressurized soaking into three steps: (1) put the coal sample into the pressurized soaking device for atmospheric pressure soaking; (2) when the coal sample is saturated under atmospheric pressure soaking conditions, remove it and place it in a plastic wrap at room temperature and away from light for 24 hr to promote the transfer of water from the surface coal body to the inside and the air out of the saturated coal sample; (3) put the coal sample into the pressurized soaking device for pressurized soaking with a pressure of 1.0 MPa.

According to the law of water absorption of the specimen, determine the saturated moisture content of the specimen and the time to reach a specific water content state. The specimens were divided into six groups, and at least nine pieces were prepared for each group. Group number W0-1-1–W0-3-3, W1-1-1–W1-3-3, W2-1-1–W2-3-3, W3-1-1–W3-3-3, W4-1-1–W4-3-3, W5-1-1–W5-3-3. W0 Group is the dry specimen, W1–W2 group moisture content is 4.0% and 8.0%, respectively; W3–W5 group is dry W3–W5 groups were one-time, two-times specimen and three-times cycle specimen. It should be noted that all saturated specimens were saturated under pressurized water immersion conditions.

The equation for determining coal samples' moisture content is shown as follows:

$$w_a = \frac{m_a - m_d}{m_d} \times 100\%, \tag{1}$$

where $w_a$ is the specimen's moisture content; $m_a$ is the specimen's mass after absorbing water; $m_d$ is the specimen's mass after drying.

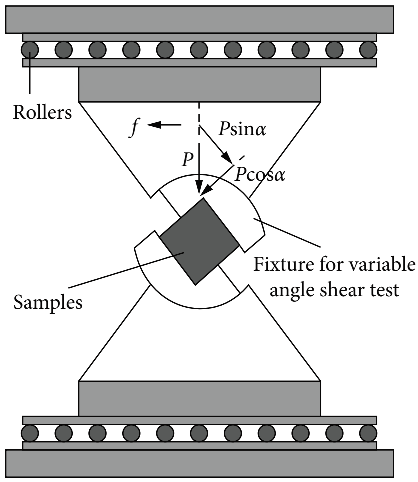


Figure 2: Shear test principle.

It should be noted that although we have tried to reduce the dispersion of coal samples by wave velocity test before the experiment, the screened coal samples still have a certain dispersion due to the complex and variable coal microcomponent, microstructure, and deposition environment, which caused important influence to the results. In addition, immersion and drying promoted the opening and development of internal cracks in coal samples, which further leads to the increase of discreteness.

The shear test and acoustic emission monitoring were performed simultaneously. The acoustic emission probe was arranged on the two exposed surfaces of the specimen. The loading was performed by displacement control with a 0.1 mm/min loading speed. As shown in Figure 2, the variable-angle shear fixture is utilized to decompose the force $P$ applied on the rock sample into shear stress $\tau$ parallel to the shear plane and normal stress $\sigma$ perpendicular to it using the following equations:

$$\sigma = \frac{F}{P}\cos\alpha, \tag{2}$$

$$\tau = \frac{F}{P}\sin\alpha, \tag{3}$$

where $\sigma$ represents the normal stress, $\tau$ represents the shear stress, $P$ is the load at the failure of the specimen, $F$ is the area of the shear plane, and $\alpha$ is the angle between the shear plane and the horizontal. Further, the $\tau - \sigma$ data were linearly fitted using the method of least squares. From this fit, the intercept on the $\tau$-axis is identified as the cohesion ($c$), and the arctangent of the slope of the line is identified as the angle of internal friction ($\varphi$).

## 3. The Water Absorption Pattern of the Sample

The water absorption process of coal samples in the atmospheric and pressurized stage is shown in Figure 3. The overall water absorption pattern of coal samples in the atmospheric soaking stage can be divided into three stages: (I) accelerated growth stage of moisture content, (II) decelerated growth stage of moisture content, and (III) saturation stage of moisture content. Similar to the atmospheric stage, the water absorption pattern of the pressurized soaked coal samples showed obvious stage characteristics and could be divided into (IV) moisture content accelerated growth stage, (V) moisture content decelerated growth stage, and (VI) moisture content saturation stage.

As shown in Figure 3, the moisture content of the coal samples reached 4.0%, 8.0%, and 10.2% (saturated moisture content under atmospheric) at 7, 26, and 120 min under atmospheric conditions, respectively. The coal samples reached 10.8% (saturated moisture content under pressurized immersion) after 150 min of continued immersion under pressurized immersion conditions. Thus, it was determined that the W1 and W2 groups of this test only went through the normal pressure process, and the immersion time was 7 and 26 min, respectively; the W3–W5 groups of coal samples will be soaked under normal pressure for 120 min and then under the pressurized stage for 180 min, and this state can be considered as reaching the saturation state.

As shown in Figure 4, there is a regular growth relationship between the moisture content of coal samples in a saturated state and the number of drying-saturation cycles. By fitting the curve, it is found that the saturated moisture content of normal pressure flooding and pressure flooding increases linearly with the increase of immersion times, and the relationship is approximately positive linear.

$$w_A = 8.780 + 0.870n \quad R^2 = 0.993, \tag{4}$$

$$w_P = 9.939 + 0.659n \quad R^2 = 0.951, \tag{5}$$

where $w_A$ and $w_P$ are the moisture content of coal samples under normal and pressurized water immersion conditions, respectively, %; $n$ is the number of immersions; $R^2$ is the correlation coefficient of the fitted curve.

According to the moisture content curves of coal samples obtained in Figures 2 and 3 under normal pressure and pressure immersion conditions, it can be seen that during the initial immersion saturation process, the changing trend of moisture content and the degree of influence of saturated moisture content of coal samples under normal pressure and pressure immersion are similar. However, under the condition of multiple dry-saturation cycles, the increase of saturated moisture content of the sample under pressure immersion is significantly greater than that under normal pressure immersion. According to Lu et al. [33], the water-containing coal sample is affected by the immersion pressure, the internal damage is aggravated, the number of pores and cracks increases, the unit water saturation of the coal sample increases, the number of pores and cracks increases, and the internal damage degree is aggravated.

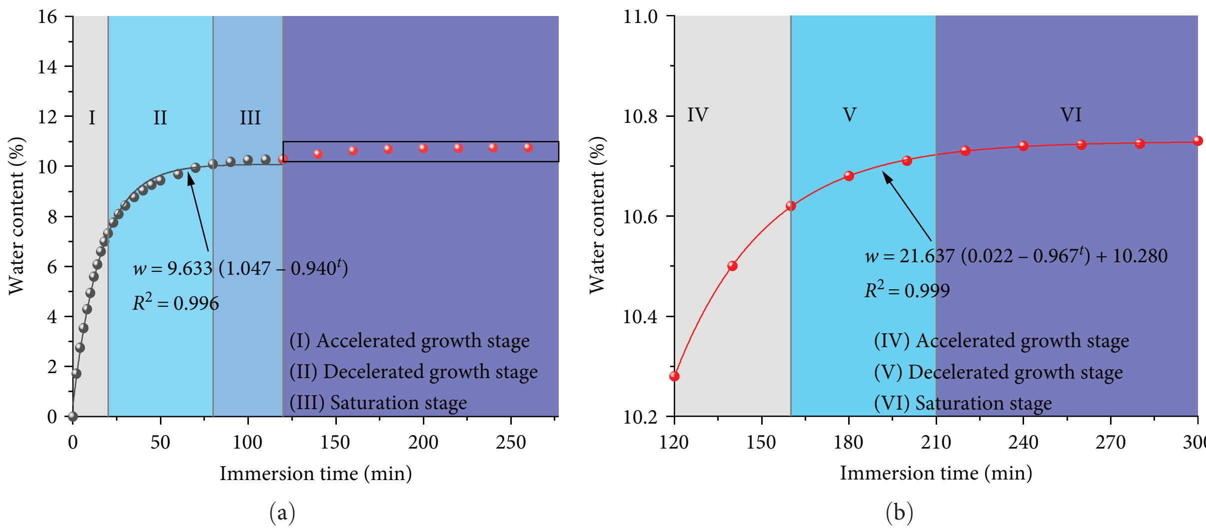


Figure 3: Immersion curve of coal sample: (a) atmospheric soaking stage; (b) pressurized soaking stage.

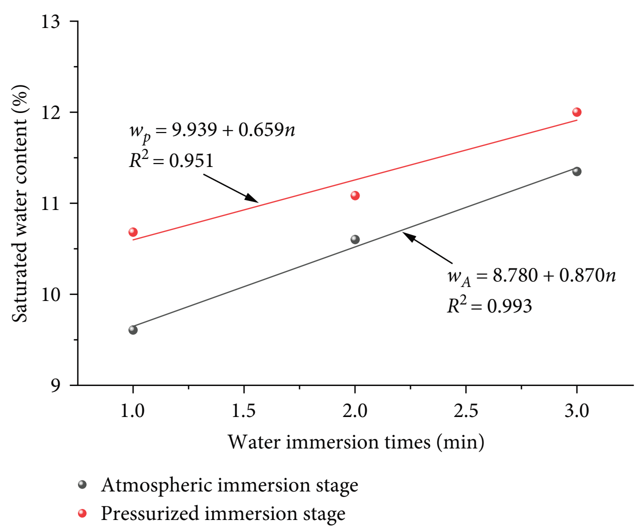


Figure 4: Relationship between moisture content and immersion times.

## 4. Weakening of Coal Sample Shear Resistance under Different Moisture Content Conditions

*4.1. Axial Load-Time Behavior of Coal Samples under Different Moisture Content Conditions.* The axial load–time curves of coal samples loaded at a 60° shear angle under different water content states are shown in Figure 5, which can be divided into five stages: (I) fracture closure stage, (II) elastic stage, (III) microfracture stable development stage, (IV) unstable rupture development stage, and (V) post-peak stage.

In the crack closure stage, the initial cracks in the specimen are gradually closed and compacted by extrusion, and the shear stress increases slowly with the increase of shear displacement. After entering the elastic stage, the initial cracks in the coal sample are closed, and the coal matrix and closed pores form a load-bearing structure, which is higher than the stiffness of the previous stage, increasing the slope of the axial load–time curve. In these two stages, the coal sample completes the closure of the initial cracks and the storage of elastic properties. In the stable development stage of cracks, the internal stress of coal samples exceeds the damage threshold of coal samples. Under increasing load, coal matrix and closed cracks are destroyed and expanded, and microcracks are stably developed in coal samples. After entering the stage of unstable fracture development, the microcracks connect and influence each other, which makes the stress structure of the specimen change constantly, resulting in several small peaks in the axial load–time curve and then reaching the main peak with the increase of load. When the coal samples' micro-cracks are connected, the final shear plane is destroyed, the stress reaches the maximum, and the coal samples enter the post-peak stage.

The degree of water damage to coal samples depends mainly on the mineral composition, structure, stress state, and other factors of coal samples. Compared with the low moisture content coal samples, the high moisture content makes the microscopic composition and structure of the coal samples change due to the damaging effect of water on the fractured coal body (mainly the weak coupling effect of hydroxide ions on the coal samples), which weakens the mechanical properties of the coal samples. As shown in Figure 5, with the increase in moisture content, the slope of the shear stress-shear displacement curve in the elastic phase decreases, and the shear modulus decreases. The duration of the fracture's stable and unstable development stages also decreases with increasing moisture content.

By comparing the axial load–time curves of coal samples with different moisture content, it can be found that the shear strength of coal samples significantly decreases with the enhancement of moisture content due to the weakening effect of water on the coal body. The shear strength of coal samples at different water content states is shown in Figure 6. When the shear angle is 65°, the shear strength of coal samples decreases from 6.08 to 2.25 MPa during the increase of moisture content from 4% to 12%, with a decrease of 63.00%;

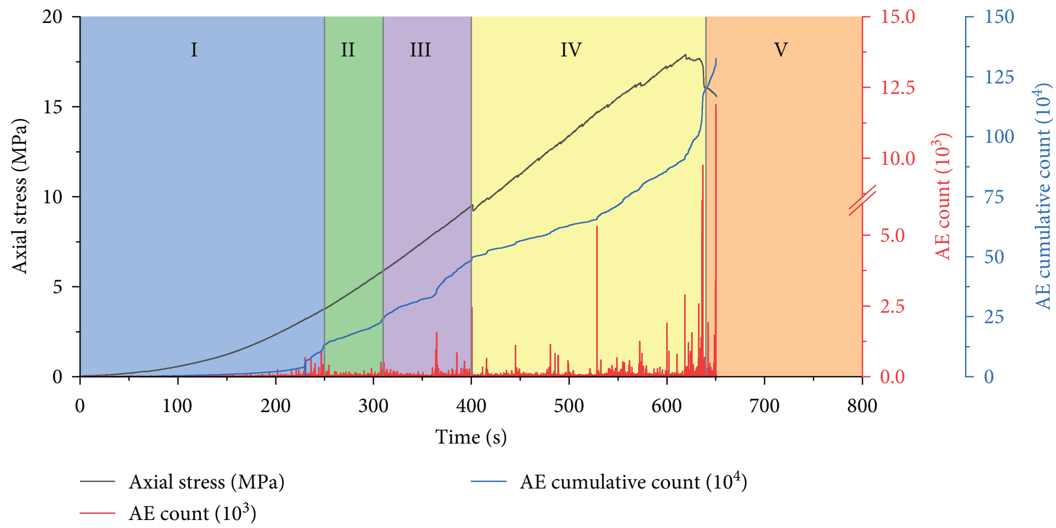


(a)

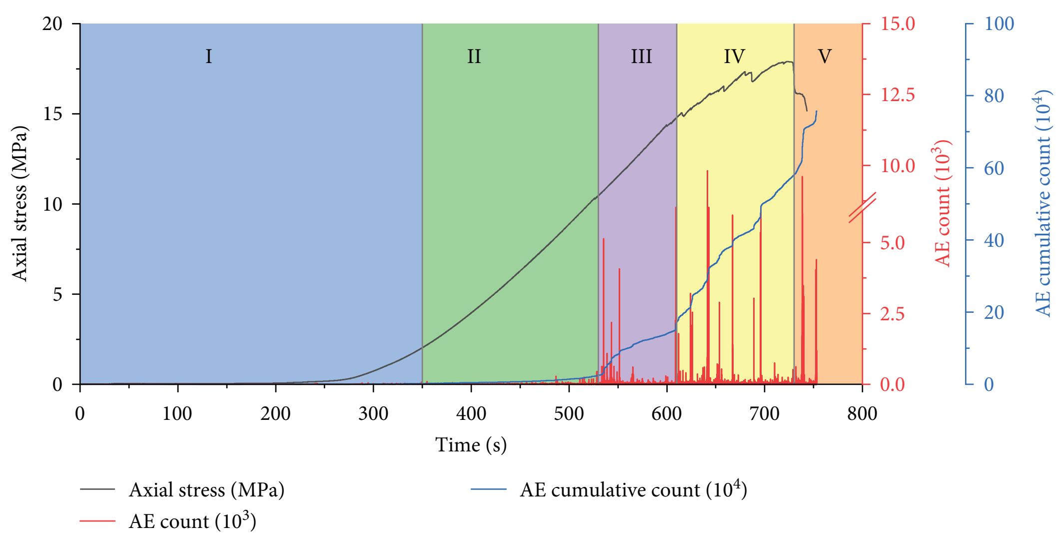


(b)

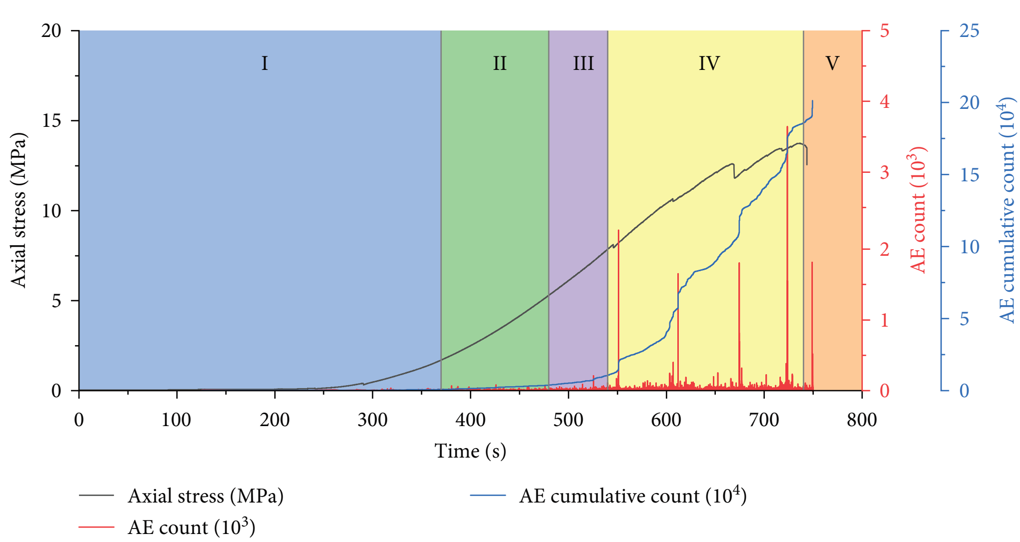


(c)

Figure 5: Continued.

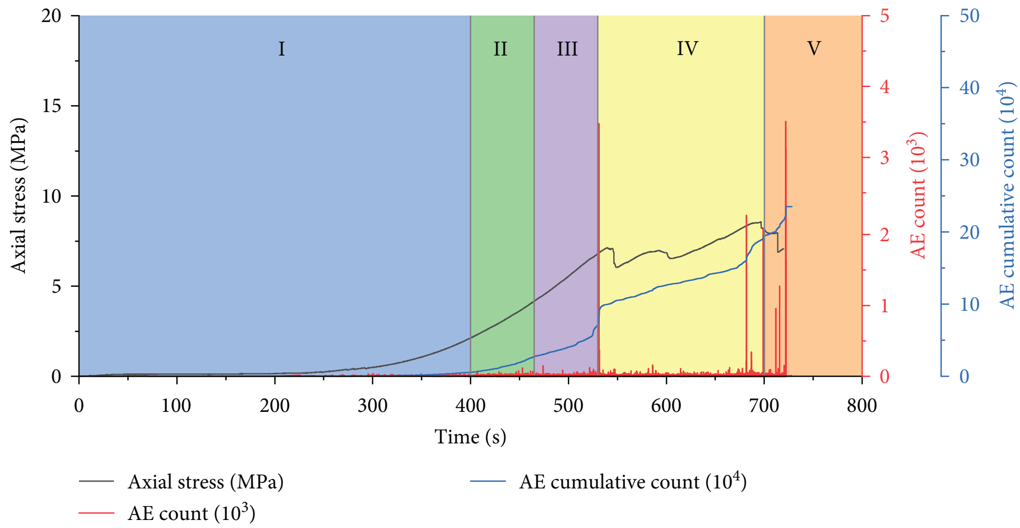


(d)

FIGURE 5: Relationship between shear strength and moisture contents: (a) W0-2-1 coal sample; (b) W1-2-1 coal sample; (c) W2-2-1 coal sample; (d) W3-2-1 coal sample.

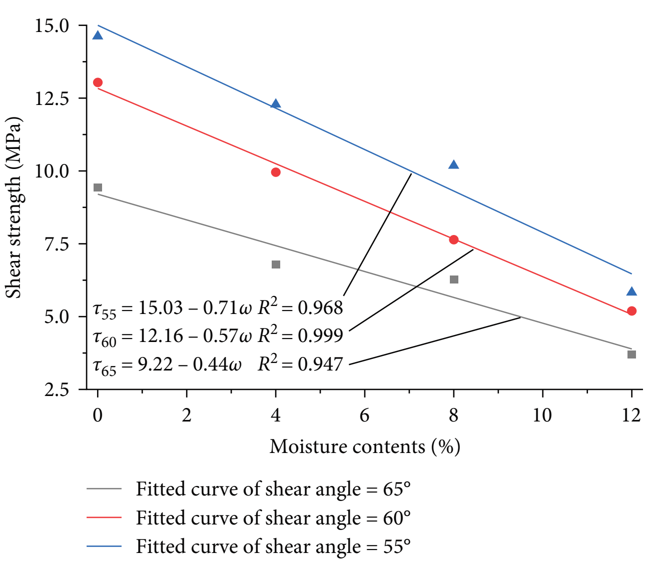


FIGURE 6: Relationship between shear strength and moisture contents.

When the shear angle is 60°, the shear strength of coal samples decreased from 11.12 to 6.42 MPa during the increase of moisture content from 4% to 12%, with a decrease of 63.00%. When the shear angle is 60°, the shear strength of coal samples decreased from 11.12 to 6.42 MPa during the increase of moisture content from 4% to 12%, with a decrease of 63.00%. The shear strength of the coal sample decreased from 11.12 to 6.42 MPa during the increase of moisture content from 4% to 12% at 60° shear angle damage, with a decrease of 42.27%. When the shear angle is 55°, the shear strength decreases from 10.68 to 5.84 MPa, during the moisture content increases from 4% to 12%, with a decrease of 45.30%. The shear strength of coal samples showed a negative linear relationship with the coal samples' moisture content and the shear angle. The fitted equations were as follows:

$$\begin{cases} \tau_{55} = 15.03 - 0.71w & R^2 = 0.968 \\ \tau_{60} = 12.16 - 0.57w & R^2 = 0.999, \\ \tau_{65} = 9.22 - 0.44w & R^2 = 0.947 \end{cases} \quad (6)$$

where $\tau_{55}, \tau_{60}, \tau_{65}$ are the specimens' shear strengths subjected to 55°, 60°, and 65° shear angle with moisture content; $x$ is the moisture content; $R^2$ is the correlation coefficient of the fitted curve.

*4.2. Acoustic Emission Characteristics of Coal Samples under Different Moisture Content Conditions.* The acoustic emission originates from inhomogeneity of granularity, primary fracture, and lattice structure inside the specimen. In the early stage of loading, the acoustic emission events are mainly due to the closure, extrusion, and misalignment of the primary fractures and pores of the coal sample, and the acoustic emission signal is relatively stable. At the later stage of loading, the acoustic emission events are due to the continued expansion of coal sample fractures, sliding friction, and penetration damage, and the acoustic emission events are more frequent and more obvious in ups and downs.

In the fracture closure stage, the primary fractures and pores of coal samples with different moisture contents start to close under the compound action of compressive and shear stresses, and the asymmetric engagement of the fracture edges and the reconstructed structure produce fewer acoustic emissions signals. Entering the elastic stage, the modulus of the coal sample approaches a constant, and the acoustic emission signal becomes active. The acoustic emission signal appears during the stable fracture development stage, but no significant peak in the count value indicates stable fracture development without large structural or stress changes. When the axial load–time curve produces the first more obvious small peak, it indicates that the coal sample enters the stage of fracture unstable development phase, producing several small peaks; the acoustic emission signal is further enhanced, and the count value is further enhanced is larger than other stages. When the axial load approaches the peak shear stress, the acoustic emission counts are relatively concentrated and produce events with larger individual counts. Compared with the dry coal samples, the acoustic emission count values and event frequencies of the water-bearing coal samples show a decreasing trend at the same stage as the moisture content increases.

Compared with the dry coal samples, the acoustic emission count values and event frequencies of the water-bearing coal samples show a decreasing trend at the same stage as the moisture content increases. From the analysis of the overall instability process of the coal sample, the acoustic emission counts of the sample with a relative moisture content of 0 decreased by 17.63%, 69.18%, and 70.32% when the moisture content increased to saturation. The cumulative count of acoustic emission decreased by 42.80%, 84.81%, and 82.22%, respectively, indicating that the plasticity and brittleness of coal samples decreased under the action of water, and this phenomenon was most obvious at the initial stage in moisture content increase, and the decline tended to be stable when the moisture content reached near saturation.

*4.3. Shear Characteristics of Coal Samples under Different Moisture Content Conditions.* The Mohr–Coulomb criterion is widely used in engineering practice. The theory holds that rock failure is mainly a shear failure related to normal and shear stress. After many experiments and mathematical analyses, it has been proved that the shear resistance of coal samples is composed of internal cohesion and internal friction angle. In the compression-shear state, the Mohr–Coulomb criterion can be used to simply and quickly determine whether the coal sample or structure occurs under a certain stress state. Shear damage. The Mohr–Coulomb strength criterion is as follows:

$$|\tau| = c + \sigma \tan\phi, \tag{7}$$

where $\tau$ is the maximum shear stress; $\sigma$ is normal stress; $c$ and $\varphi$ are the internal cohesion and internal friction angle, which could be obtained by variable angle shear test according to recommendations from the National Standard of the People's Republic of China (GB/T 23561.11-2010).

Internal cohesion and internal friction angle are important parameters to evaluate the shear performance of coal in engineering design. The mutual attraction between the molecules within the material is internal cohesion, which promotes molecular polymerization into a whole. The angle of internal friction is a common concept of sliding and occlusal friction. Therefore, in the process of specimen failure, the internal cohesion is closely related to the generation of cracks, and the internal friction angle is related to the expansion, dislocation, and failure of cracks, so it is widely used to

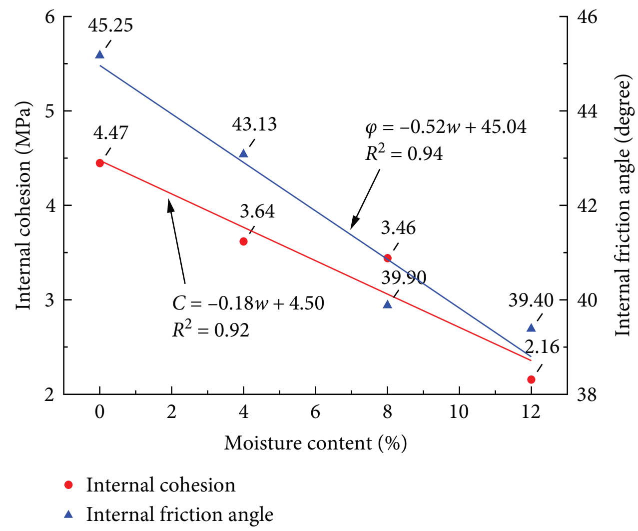


Figure 7: Relationship between internal cohesion, internal friction angle, and moisture contents.

evaluate the mechanical properties of the engineering rock mass. The change of internal cohesion and internal friction angle of the sample under different moisture content is shown in Figure 7.

With the increase of moisture content, coal samples' internal cohesion force and internal friction angle showed a linearly decreasing trend. When the moisture content is 0%, the internal cohesion force and the internal friction angle are 4.47 MPa and 45.25°, respectively, and they reach 2.16 MPa and 39.40° in the saturated state, with a decrease of 51.68% and 12.93%, respectively. Because the coal sample must overcome the occlusal friction generated by the motion of embedded, connected, and separated particles, the sliding friction generated by the rough surface of the particles before the compressive shear damages the sample. For coal samples with high moisture content, water not only enters the crystal lattice of the coal sample, weakening the bonds of the original structure inside the coal, thereby changing the microstructure of the coal and reducing the internal cohesion of the coal; lubrication of the fracture surfaces reduces the angle of internal friction, thereby reducing the strength of the sample. Based on this, the Mohr-Coulomb model of coal samples with any moisture content is established, as shown in the following equation:

$$|\tau| = (-0.18w + 4.50) + \sigma \cdot \tan(-0.52w + 45.04). \tag{8}$$

## 5. Weakening of Coal Sample Shear Resistance under Different Water Immersion Times

*5.1. Axial Load-Time Behavior of Coal Samples under Different Water Immersion Times.* Figure 8 shows the axial load–time curves of coal samples under 60° shear angle loading under different water immersion times.

Compared with the three groups of unsaturated samples in the previous section, the damage and destruction process

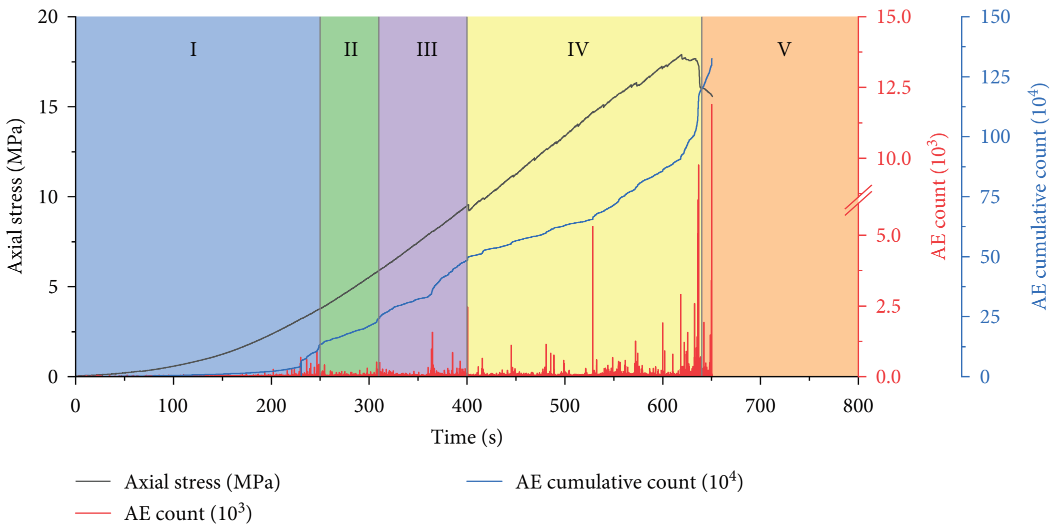


(a)

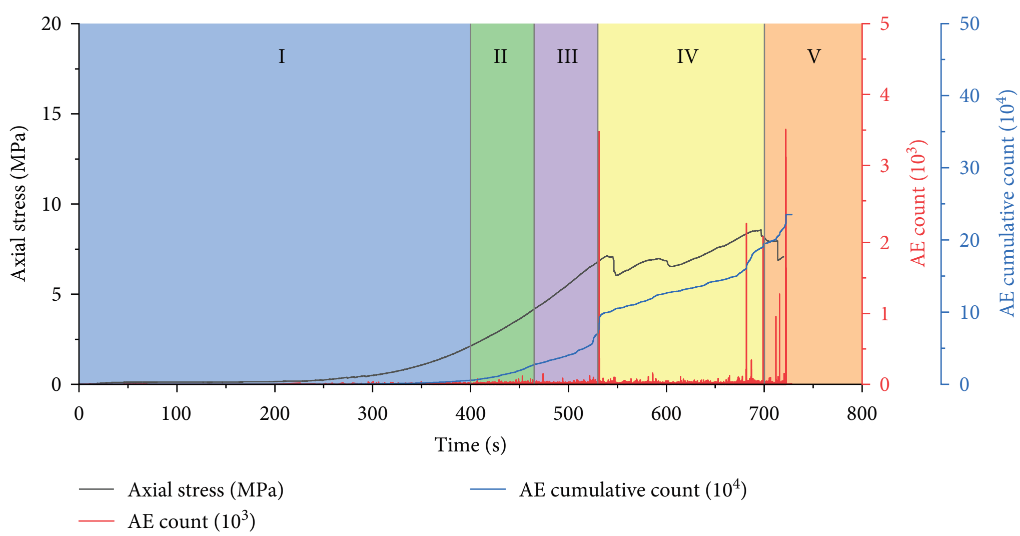


(b)

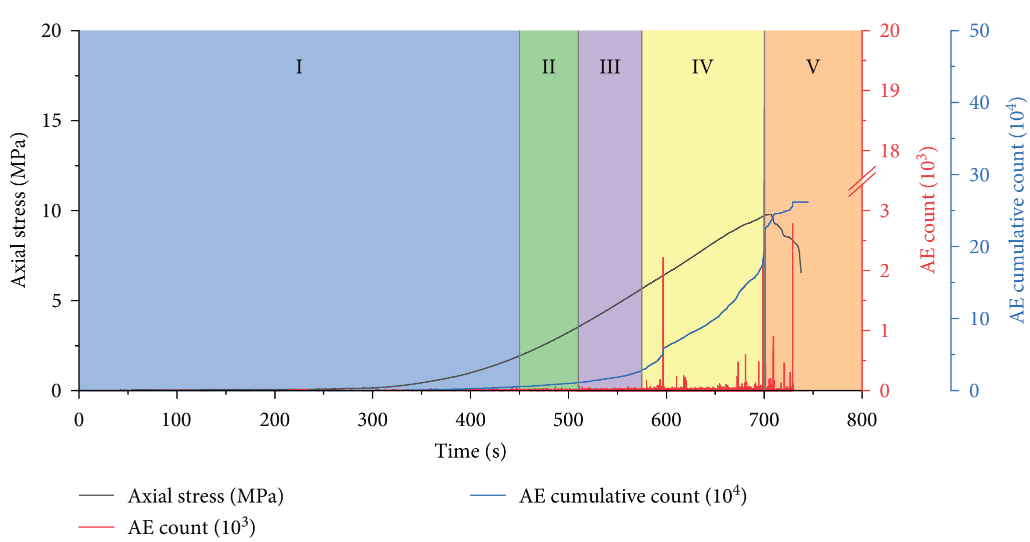


(c)

Figure 8: Continued.

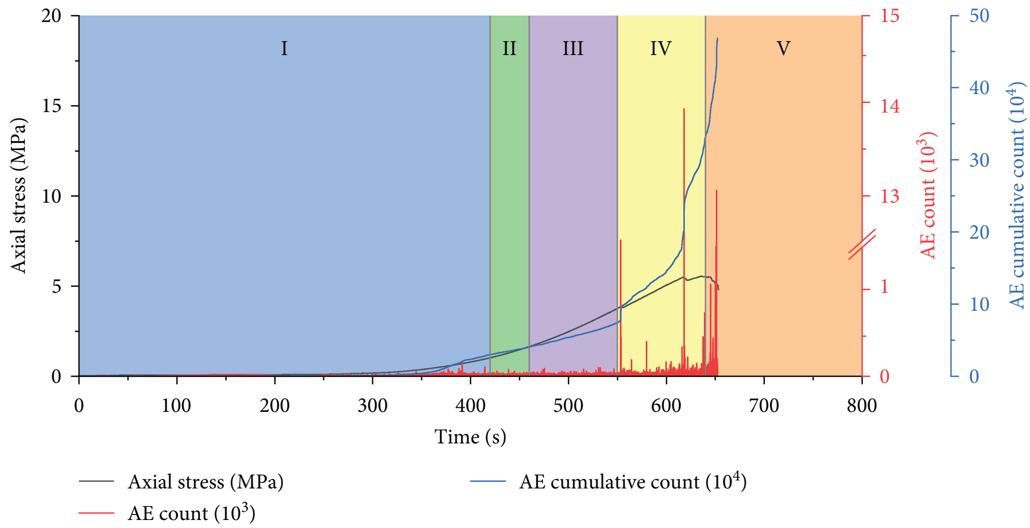


(d)

Figure 8: Relationship between shear strength and immersion times: (a) W0-2-1 coal sample; (b) W1-2-1 coal sample; (c) W2-2-1 coal sample; (d) W3-2-1 coal sample.

of the dry-saturated samples is less severe, the AE cumulative count curves in the elastic stage and the stable development stage of the cracks rise slowly, and the cracks are unstable in the development stage. The high count value is fewer. The drying-saturation cycle process makes the clay minerals expand to fill the pores and fracture spaces of the coal sample, and the stress is distributed more evenly during loading, causing plastic deformation and driving fracture expansion. After reaching the peak stress, the saturated sample with strong plastic deformation ability will not be destroyed but will continue to be gradually destroyed by the action of force.

After reaching the peak stress, the saturated sample with strong plastic deformation ability will not be destroyed but will continue to be gradually destroyed by the action of force. According to the AE cumulative counting characteristics, the total response degree of the sample decreases significantly with the increase of the number of dry-saturation times, and the reduction degree of one dry-saturation is the highest, 82.22%. The subsequent reduction degree is slightly lower, 80.23% and 64.62%, indicating that the dry-saturation treatment will increase the brittleness of the sample to a certain extent, and the increasing degree is affected by the combination of the number of cycles and the natural cracks in the sample.

By comparing the axial load-time curves of coal samples under different cycles, it can be found that due to the irreversible damage to the coal body caused by the drying-saturation cycle process, the shear strength of the coal samples decreases significantly with the increase of moisture content. The shear strength of coal samples under different cycle times is shown in Figure 9. When the shear angle is 65°, the coal sample shear strength decreases from 3.70 to 3.02 MPa during the immersion cycle, increases from 1 to 3 times, and the decrement is 18.38%. When the shear angle is 60°, the coal sample shear strength decreases from 5.20 to 3.55 MPa as the immersion cycle increases from 1 to 3 times, and

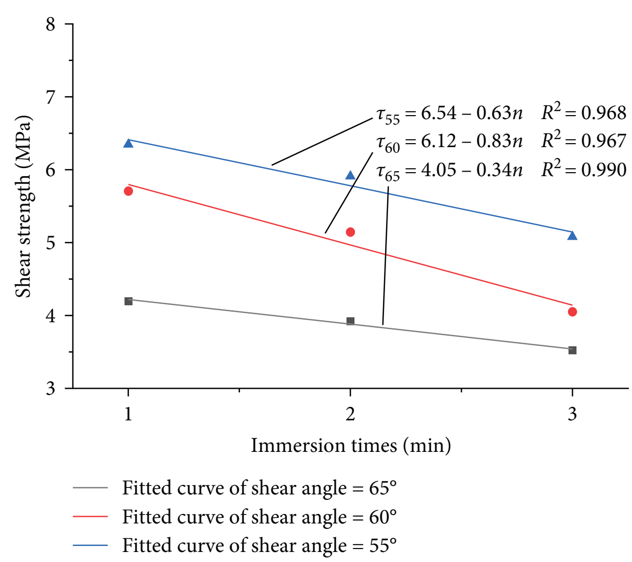


Figure 9: Relationship between shear strength and immersion times.

the decrement is 31.73%. When the shear angle is 55°, the coal sample shear strength decreases from 5.84 to 4.58 MPa as the immersion cycle increases from 1 to 3 times, and the decrement is 21.57%.

Under the three shearing angles, the relationship between the specimens' shear strength and the immersion cycle times was consistent, and the shear strength decreased linearly with the increase of the cycle times. The fitting equation between the shear strength of coal samples and the number of immersion times is shown in Equation (7). During the repeated drying-saturation cycle cycles, clay minerals and other minerals are continuously dissolved and transferred, the microstructure is constantly changed, and the local load-bearing structure is seriously damaged.

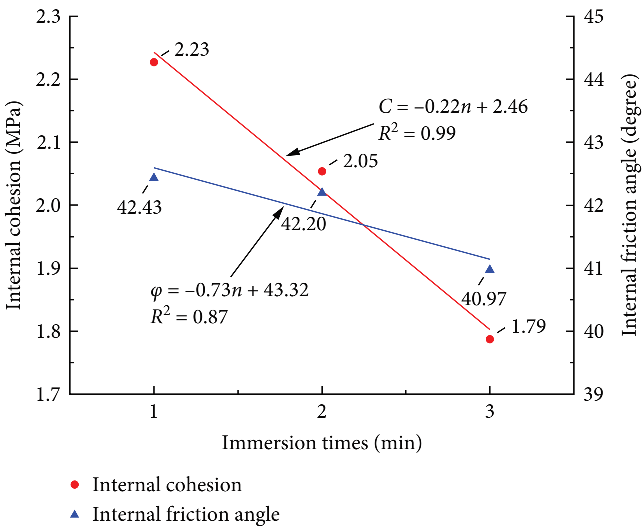


Figure 10: Relationship between internal cohesion, internal friction angle, and immersion times.

$$\begin{cases} \tau_{55} = 6.54 - 0.63n & R^2 = 0.968 \\ \tau_{60} = 6.12 - 0.83n & R^2 = 0.967, \\ \tau_{65} = 4.05 - 0.34n & R^2 = 0.990 \end{cases} \tag{9}$$

where $n$ is the immersion cycle times.

*5.2. Shear Characteristics of Coal Samples under Different Water Immersion Times.* As shown in Figure 10, with the increase in water immersion times, the coal sample's internal cohesion and internal friction angle both show a linear downward trend. The fitting functions were as follows:

$$\begin{array}{ll} C = -0.22n + 2.46 & R^2 = 0.99 \\ \phi = -0.73n + 43.32 & R^2 = 0.87 \end{array}. \tag{10}$$

As the immersion increased from 1 to 3 times, the internal cohesion decreased from 2.23 to 1.79 MPa, 19.73%. Water molecules penetrate the micropores inside the coal sample after entering the sample and form a water film between the coal particles, which weakens the internal cohesion between the microstructures and reduces the internal cohesion that needs to be overcome during failure. With the cycle times increased, the continuous dissolution and transfer of clay minerals and other minerals resulted in the further infiltration of water into the pores of the coal sample, resulting in a decrease in the internal cohesion of the coal sample with the increase of the number of cycles. At the same time, clay minerals and other minerals are continuously dissolved and transferred, the structure of the coal sample changes, and the degree of physical weakening increases with the increase of the number of cycles, resulting in a decrease in the internal friction angle. As the immersion increased from 1 to 3 times, the internal friction angle decreased from 42.30° to 40.97°, decreasing by 3.14%.

Taking Equation (8) into the Mohr–Coulomb strength criterion, the relationship between the shear strength and the immersion cycle times can be obtained as follows:

$$|\tau| = (-0.22n + 2.46) + \sigma \tan(-0.73n + 43.32). \tag{11}$$

According to Equation (9), it can be found that with the increase of water immersion times, the internal cohesion and internal friction angle of coal samples decreases, and the corresponding macroscopic intermolecular forces and frictional forces that need to be overcome become smaller, which is more prone to damage.

*5.3. Mohr–Coulomb Criterion Considering Water-Bearing State.* According to Equations (6) and (9), the number of dry-saturation cycles and the increase of moisture content will affect the cohesion and internal friction angle of coal samples and then change the form of the Mohr–Coulomb criterion. A unified general equation is established based on the impact of the above two cases, which can be expressed as follows:

$$|\tau| = (R_1 f_\omega + c_0) + \sigma \tan(R_2 f_\omega + \varphi_0). \tag{12}$$

In the equation, $c_0$ and $\phi_0$ represent the cohesion and internal friction angle of the sample in the anhydrous state without the effect of the dry-saturation cycle, and $R_1$ and $R_2$ are the influence coefficients of the water rock interaction condition on the cohesion and internal friction angle, which are both negative values, reflecting the weakening effect of moisture content and dry-saturation cycle on the cohesion and internal friction angle.

## 6. Discussion

The research results mentioned above indicate that the water content states (moisture content and dry-saturation cycling) of coal samples significantly affect their mechanical properties. To further deeper into the damage mechanisms of coal samples under different moisture conditions, SEM analysis was conducted on coal samples with varying moisture levels. Figure 11 shows SEM images of coal samples magnified 1,000 times under different moisture conditions, revealing significant changes in their microstructure: as the moisture content and dry-saturation cycles increase, the microstructure of the coal samples gradually shifts from orderly and compact to disordered and murky, with notable changes in the size, shape, and distribution of pores.

Specifically, as shown in Figure 11(a), dry coal samples have rough surfaces with abundant depressions and protrusions, forming a layered accumulation with a larger specific surface area conducive to liquid adsorption. At a moisture content of 4.0%, as depicted in Figure 11(b), various physical and chemical effects such as lubrication, liquefaction, ion exchange, and mineral dissolution occur upon contact with water, leading to the formation of multiple erosion holes on the coal sample surface. When the moisture content reaches 8.0%, as shown in Figure 11(c), more erosion holes appear on

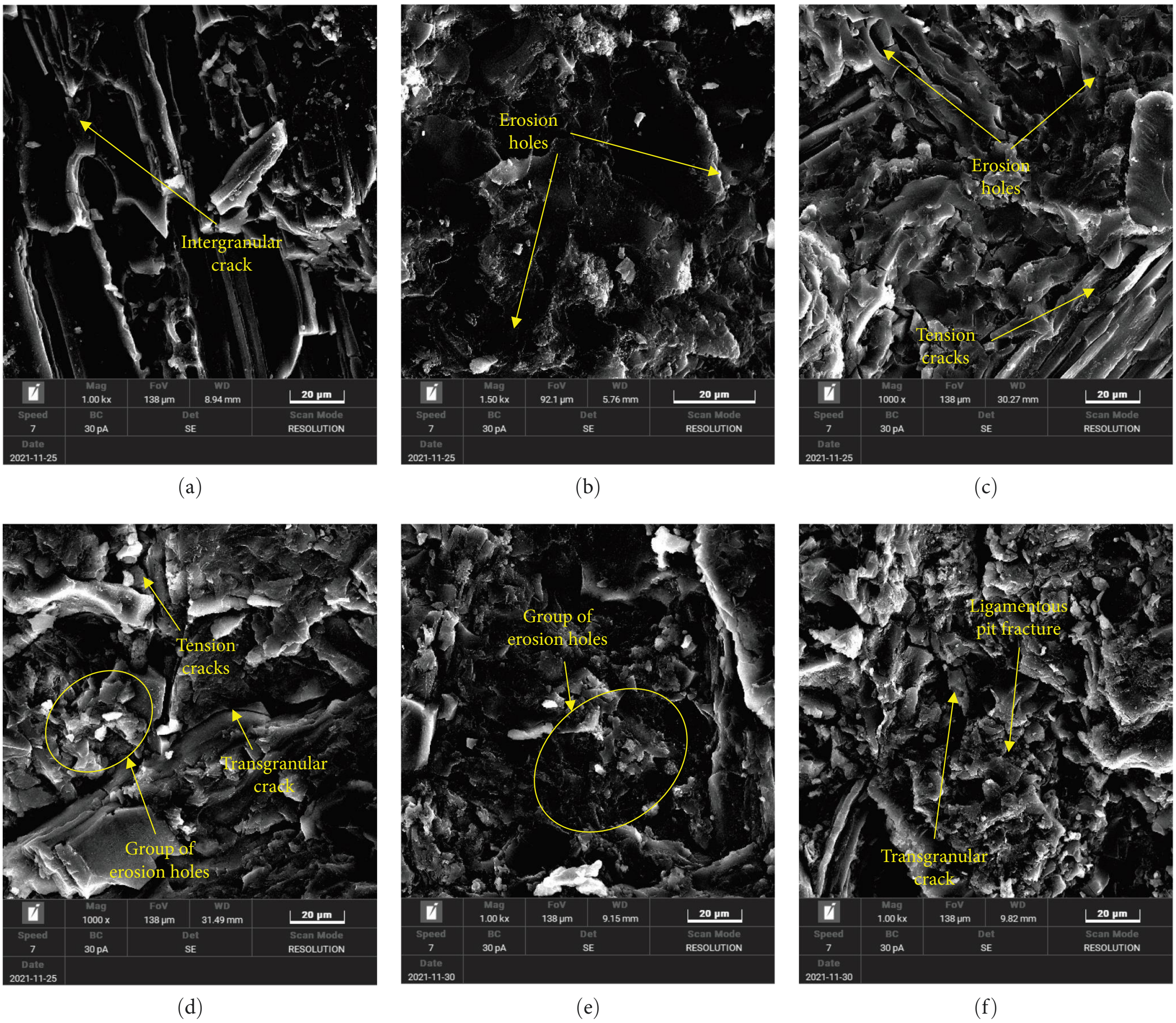


FIGURE 11: SEM images of coal samples under various water content states: (a) $w_a = 0.0\%$; (b) $w_a = 4.0\%$; (c) $w_a = 8.0\%$; (d) one-time cycle; (e) two-times cycle; (f) three-times cycle.

the surface due to increased hydration reactions of clay minerals in the coal sample components. Moreover, the abundance of erosion holes weakens the matrix's fracture strength, leading to the initiation of tensile cracks under the influence of the expansion force generated by the absorption of water by clay minerals. When the coal sample reaches a saturated state, as illustrated in Figure 11(d), a densely populated group of erosion holes begins to appear on the coal sample's surface, significantly deteriorating the mechanical structure of the coal matrix and enhancing the heterogeneity of the microstructure, further promoting the development and enlargement of tensile cracks in the coal sample. Furthermore, as shown in Figures 11(e) and 11(f), under the effect of dry-saturation cycles, the number and size of erosion holes and microcracks in the observed area of the coal sample increase significantly, making it more prone to the formation of tensile fissures and further weakening the mechanical performance of the coal sample. Additionally, due to the promotion of clay minerals and coal fragments precipitating from the coal matrix during the dry-saturation cycle, as the number of dry-saturation cycles increases, erosion holes further dissolve and communicate with each other, forming ligamentous pit fractures.

Summarizing the mechanisms through which different water content states weaken the mechanical performance of coal samples, it can be broadly attributed to the following two aspects [34–38]:

(1) The presence of water within the samples weakens the internal friction of the matrix. When subjected to external loads, the rock tends to slide along fractures. Additionally, as water molecules are polar, they readily engage in oxidation–reduction interactions with the rock matrix, resulting in the formation of weaker secondary minerals, thereby reducing the strength of

the samples. Moreover, the expansion force generated by the absorption of water by clay minerals in the samples promotes the further development of cracks.

(2) The ingress of water into pores and fractures increases pore pressure, leading to a reduction in effective stress within the coal. This, in turn, weakens the fracture strength of the matrix and diminishes the overall mechanical strength of the specimens. Simultaneously, the presence of free water within the fractures causes stress concentration at the tips, promoting the further expansion and enlargement of internal cracks.

(3) During the drying-saturation cycle, the absorption of water causes the coal body to expand, while the drying process leads to its contraction. This continuous cycle of expansion and contraction can lead to the formation and expansion of microcracks, weakening the overall structural strength of the coal. Additionally, the absorption and release of heat within the coal body occur. This thermodynamic effect can cause thermal expansion and contraction of the materials inside the coal body, further affecting its mechanical properties.

## 7. Conclusion

(1) The coal samples in the atmospheric stage and the pressure stage, the coal samples showed similar water absorption laws, which can be divided into three stages according to the moisture content growth rate: (I) the accelerated growth stage, (II) the decelerated growth stage, and (III) the saturation stage.

(2) The variation law of shear strength of coal samples with moisture content and drying-saturation cycles under different shear angles is consistent. The shear strength of coal samples decreased not only with the increase of moisture content but also with the drying-saturation cycles of coal samples. This result will help to further reveal the weakening effect of water immersion and drying process on the mechanical properties of coal samples.

(3) The evolution of internal cohesion and internal friction angle of coal samples with moisture content and drying-saturation cycle times are similar. With the increase of moisture content or drying-saturation cycle times, coal samples' internal cohesion and internal friction angle showed a decreasing trend. Furthermore, the Mohr–Coulomb criterion was modified by considering the influence of moisture content and drying-saturation cycle times, which could contribute to the estimation of the load-bearing capacity of water-bearing coal mass.

(4) Additionally, SEM analysis has revealed significant changes in the microstructure of coal samples under various moisture states: as moisture content and the number of drying-saturation cycles increases, the microstructure of coal samples shifts from being orderly and compact to disordered and murky, with notable changes in the size, shape, and distribution of pores. These alterations in microstructure reflect the mechanisms by which moisture weakens the mechanical properties of coal samples.

It should be noted that this study provided some insights about coal water-resistant capacity in the field of coal mining as well as an experimental dataset of coal sample shear characteristics in different water-bearing states. However, The tests and analyses in this study were based on coal samples acquired from the Shendong Mining Area in Inner Mongolia. Further studies are required to investigate the effects of coal type, strength, and special solution on the shear characteristics of coal samples in different water-bearing states. Moreover, factors such as immersion water pressure and drying temperature can affect the experimental results; therefore, higher immersion water pressure and higher drying temperature should also be added to the scope of further research in the future. We will conduct studies to address these limitations in our subsequent work with the hope of providing useful references for engineering problems related to the stability evaluation of coal bodies involving the repeated erosion effect of water.

## Data Availability

Data available on request due to restrictions, e.g., privacy or ethical.

## Conflicts of Interest

The authors declare that they have no conflicts of interest.

## Authors' Contributions

Conceptualization was done by Y.W. and B.W.; methodology was done by Y.W. and L.W.; software-related task was done by Z.X.; formal analysis was performed by X.X.; investigation was done by Y.W. and B.W.; resources were provided by Z.X.; data curation was done by L.W.; writing—original draft preparation was done by Y.W.; writing—review and editing was done by B.W., L.W., and Z.X.; visualization was done by Z.X.; project administration was done by B.W.; funding acquisition was made by Y.W. All authors have read and agreed to the published version of the manuscript.

## Acknowledgments

This research was funded by the National Natural Science Foundation of China (grant number 52004011) and the National Energy Group Science and Technology Innovation Project (grant number GJNY-18-80).

## References


[1] Y. Zhang, Y. Liu, X. Lai et al., "Transport mechanism and control technology of heavy metal ions in gangue backfill materials in short-wall block backfill mining," *Science of the Total Environment*, vol. 895, Article ID 165139, 2023.

[2] L. Fan and X. Ma, "A review on investigation of water-preserved coal mining in western China," *International Journal of Coal Science & Technology*, vol. 5, pp. 411–416, 2018.

[3] L. M. Fan, "Scientific connotation of water-preserved mining," *Journal of China Coal Society*, vol. 42, no. 1, pp. 27–35, 2017.

[4] D. Z. Gu, "Theory framework and technological system of coal mine underground reservoir," *Journal of China Coal Society*, vol. 40, no. 2, pp. 239–246, 2015.

[5] L. M. Fan, X. D. Ma, Q. Y. Wu et al., "Analysis on technical points of water-preserving coal mining technical specifications," *Coal Science and Technology*, vol. 48, no. 9, pp. 81–87, 2020.

[6] L. M. Fan, X. D. Ma, Z. Q. Jiang, K. Sun, and R. J. Ji, "Review and thirty years prospect of research on water-preserved coal mining," *Coal Science and Technology*, vol. 47, no. 7, pp. 1–30, 2019.

[7] D. Z. Gu, T. Li, J. F. Li et al., "Current status and prospects of coal mine water treatment technology in China," *Coal Science and Technology*, vol. 49, no. 1, pp. 11–18, 2021.

[8] D. Z. Gu, Y. Zhang, and Z. G. Cao, "Technical progress of water resource protection and utilization by coal mining in China," *Coal Science and Technology*, vol. 44, no. 1, pp. 1–7, 2016.

[9] D. Z. Gu, J. F. Li, Z. G. Cao et al., "Technology and engineering development strategy of water protection and utilization of coal mine in China," *Journal of China Coal Society*, vol. 46, no. 10, pp. 3079–3089, 2021.

[10] C. J. Tang, Q. L. Yao, W. N. Wang, and X. H. Wang, "Experimental study on damage characteristics of sandy mudstone under the action of water," *Journal of China Coal Society*, vol. 44, no. 3, pp. 882–890, 2019.

[11] D.-S. Zhang, W.-P. Li, X.-P. Lai, G. W. Fan, and W.-Q. Liu, "Development on basic theory of water protection during coal mining in northwest of China," *Journal of China Coal Society*, vol. 42, no. 1, pp. 36–43, 2017.

[12] Q. L. Yao, T. Chen, X. H. Li, and A. Wang, "Experimental study on coarsely water-bearing sandstone in roof of Jurassic coal seam," *Journal of China Coal Society*, vol. 42, no. 1, pp. 183–188, 2017.

[13] X.-H. Li, S. Liang, Q.-L. Yao, Q.-D. Ju, and L. Zhang, "Analysis on fissure-evolving law and roof-falling mechanism in roadway with mudstone roof," *Journal of China Coal Society*, vol. 36, no. 6, pp. 903–908, 2011.

[14] Q. L. Yao, W. N. Wang, S. Y. Yang, J. Fang, and B. J. Zhou, "Direct shear and acoustic emission characteristics of sandy mudstone under the effect of moisture content," *Journal of China Coal Society*, vol. 46, no. 9, pp. 2910–2922, 2021.

[15] Y. Xue, P. G. Ranjith, F. Gao, Z. Zhang, and S. Wang, "Experimental investigations on effects of gas pressure on mechanical behaviors and failure characteristic of coals," *Journal of Rock Mechanics and Geotechnical Engineering*, vol. 15, no. 2, pp. 412–428, 2023.

[16] T. Chen, Q.-L. Yao, F. Wei et al., "Effects of water intrusion and loading rate on mechanical properties of and crack propagation in coal–rock combinations," *Journal of Central South University*, vol. 24, pp. 423–431, 2017.

[17] Z. Zhao, W. Wang, L. Wang, and C. Dai, "Compression–shear strength criterion of coal–rock combination model considering interface effect," *Tunnelling and Underground Space Technology*, vol. 47, pp. 193–199, 2015.

[18] S. Heng, C. H. Yang, Y. J. Ceng et al., "Anisotropy of shear strength of shale based on direct shear test," *Chinese Journal of Rock Mechanics and Engineering*, vol. 33, no. 5, pp. 874–883, 2014.

[19] Z.-H. Zhou, P. Cao, and Z.-Y. Ye, "Crack propagation mechanism of compression-shear rock under static–dynamic loading and seepage water pressure," *Journal of Central South University*, vol. 21, pp. 1565–1570, 2014.

[20] J. Xu, L. F. Lu, H. W. Yang, Y. Zhang, and L. Wang, "Study of evolution law of microfracturing progress of sandstone under shear loading," *Chinese Journal of Rock Mechanics and Engineering*, vol. 30, no. 5, pp. 944–950, 2011.

[21] K. G. Li, K. P. Hou, and C. L. Zhang, "Experiment study on shear characteristics of saturated rock mass," *Journal of Central South University (Science and Technology)*, vol. 40, no. 2, pp. 538–542, 2009.

[22] C. Q. Chu, S. C. Wu, Z. S. Cao, C. J. Zhang, and Y. L. Zhang, "Experimental research on fracture characteristics of granite with acoustic emission technology," *Journal of Central South University (Science and Technology)*, vol. 52, no. 8, pp. 2919–2932, 2021.

[23] K. Li, K. Hou, and C. Zhang, "Experimental study of fractal dimension of AE serials of different rocks under uniaxial compression," *Rock and Soil Mechanics*, vol. 33, no. 12, pp. 3561–3569, 2012.

[24] D. H. Yang, Y. X. Zhao, T. Teng et al., "Study on critical characteristics of acoustic emission in sandstone fracture instability and Kaiser point recognition," *Journal of Basic Science and Engineering*, vol. 29, no. 1, pp. 218–230, 2021.

[25] Q. Sun, L. Xue, and S.-Y. Zhu, "Analysis of critical acoustic emission information of sandstone brittle failure with stress ratio," *Rock and Soil Mechanics*, vol. 33, no. 9, pp. 2575–2580, 2012.

[26] X. L. Liu, M. C. Pan, X. B. Li, and J. P. Wang, "Acoustic emission b-value characteristics of granite under dynamic loading and static loading," *Chinese Journal of Rock Mechanics and Engineering*, vol. 36, no. S1, pp. 3148–3155, 2017.

[27] Y. F. Zhao, L. Q. Liu, Y. S. Pan, B. B. Jiao, and C. Zhang, "Experiment study on microseismic, charge induction, self-potential and acoustic emission during fracture process of rocks," *Chinese Journal of Rock Mechanics and Engineering*, vol. 36, no. 1, pp. 107–123, 2017.

[28] M. Wang, C. Tan, J. Meng, B. Yang, and Y. Li, "Crack classification and evolution in anisotropic shale during cyclic loading tests by acoustic emission," *Journal of Geophysics and Engineering*, vol. 14, no. 4, pp. 930–938, 2017.

[29] Y. Xue, S. Liu, J. Chai et al., "Effect of water-cooling shock on fracture initiation and morphology of high-temperature granite: application of hydraulic fracturing to enhanced geothermal systems," *Applied Energy*, vol. 337, Article ID 120858, 2023.

[30] X. Gao, S. J. Liu, J. W. Huang, Z. C. Yang, W. F. Mao, and L. X. Wu, "The influence of strain rate on AE characteristics during rock deformation," *Chinese Journal of Rock Mechanics and Engineering*, vol. 37, no. 4, pp. 887–897, 2018.

[31] S.-C. Wu, C. Guo, Y. T. Gao, C. J. Zhang, and F. R. Zheng, "Discussion and prospect of source location of rock fracture," *Chinese Journal of Rock Mechanics and Engineering*, vol. 40, no. 5, pp. 874–891, 2021.

[32] J. Xu, Y. Liu, and S. Peng, "Acoustic emission parameters of Three Gorges sandstone during shear failure," *Acta Geophysica*, vol. 64, pp. 2410–2429, 2016.

[33] L. Yu, Q. Yao, Z. Chong, Y. Li, Q. Xu, and Z. Liu, "Experimental study on the moisture migration and triaxial mechanical damage mechanisms of water-bearing coal samples," *International Journal of Rock Mechanics and Mining Sciences*, vol. 160, Article ID 105263, 2022.

[34] K. Bian, J. Liu, W. Zhang, X. Zheng, S. Ni, and Z. Liu, "Mechanical behavior and damage constitutive model of rock subjected to water-weakening effect and uniaxial loading," *Rock Mechanics and Rock Engineering*, vol. 52, pp. 97–106, 2019.

[35] X. Liu, M. Jin, D. Li, and L. Zhang, "Strength deterioration of a Shaly sandstone under dry–wet cycles: a case study from the Three Gorges Reservoir in China," *Bulletin of Engineering Geology and the Environment*, vol. 77, pp. 1607–1621, 2018.

[36] L. Si, J. Wei, Y. Xi et al., "The influence of long-time water intrusion on the mineral and pore structure of coal," *Fuel*, vol. 290, Article ID 119848, 2021.

[37] Q. Jiang, J. Cui, X. Feng, and Y. Jiang, "Application of computerized tomographic scanning to the study of water-induced weakening of mudstone," *Bulletin of Engineering Geology and the Environment*, vol. 73, pp. 1293–1301, 2014.

[38] C. Zheng, Q. Yao, X. Li et al., "Evolution law of ultrasonic characteristics and its relationship with coal-measure sandstone mechanical properties during saturation and desaturation," *Journal of Building Engineering*, vol. 75, Article ID 106909, 2023.